Chapter 4

Fabrication and Characterization of ZnO CQDs/ F8BT Heterojunction-based UV-Visible Photodetectors With/Without MoOx HTL

- .

***Part of this work has been published as:**

Abhinav Pratap Singh and S. Jit, "Performance Optimization of ZnO QDs/F8BT Heterojunction-Based UV–Visible Photodetectors Using MoOx Hole Transport Layer," ***IEEE Transactions on Electron Devices,*** (Early Access) 26 June 2013 Doi: 10.1109/TED.2023.3285717.

Chapter 4

Fabrication and Characterization of ZnO CQDs/ F8BT Heterojunction-based UV-Visible Photodetectors With/Without MoOx HTL

4.1. Introduction

The performance improvement in UV photodetectors have been achieved using TIPS-pentacene in Chapter-2 and Chapter-3. In this chapter, the detection wavelength is increased to visible range by replacing TIPS-pentacene with visible light sensitive. This extended wavelength range photodetector is classified as ultraviolet-visible (UV-Vis) photodetector. UV-Vis photodetectors are broadly used in air pollution control, optical communication, environment monitoring, biomedical imaging, ultraviolet astronomy, wide spectral switches and memory storage applications [94][81]. To obtain the UV-visible photodetectors, several researchers have explored inorganic-organic heterojunctions formed between ZnO and an organic semiconductor such as F8BT [1][95], PEDOT:PSS [96], PTB7 [97][98], PCBM [99], poly(N-vinyl carbazole) (PVK) [29], and Poly (3-hexylthiophene-2, 5-diyl) (P3HT). Among various organic polymers mentioned above, F8BT has shown better optoelectronic characteristics [100], [101]. It is a conjugated copolymer derivative of polyfluorene that has benzothiadiazole as the electron-acceptor unit and fluorene as the electron donor. It is an electron donor-acceptor, p-type semiconductor. Moreover, F8BT exhibits robust stacking interactions, efficient charge-carrier transport, and improved electrical conductivity because delocalized electrons are present in the conjugated polymer's backbone. [102], [103]. Further improvement in photodetection characteristics is achievable through the minority carrier blocking interfacial layer as achieved in previous chapter and discussed in literature in Chapter-1.

In this chapter, section 4.2 represents the basic steps involved in fabrication of photodetector along with device structure and band diagram whereas the section 4.3 outlines the basic absorbance and photoluminescence study of the various films and their combination followed by optoelectronic characterization of the fabricated device. Subsequently section 4.4 quickly summarizes the obtained results.

4.2. Experimental Details

The UV-Vis photodetectors were fabricated on ITO-coated glass substrate. Cleaned ITO-coated glass substrates of 15 mm × 15 mm size were processed for Ar-O_2 plasma (ratio of 20 %: 20 %) cleaning using Femto Science Inc. CUTE, Korea with 80 W power and 60 Hz frequency for 10 minutes. Thin film of the as-synthesized ZnO CQDs was grown on the ITO-coated glass substrates using spin coating method (SPM-150LC TSE-system GmbH, Germany) at 2000 rpm for 45 sec followed by low temperature annealing at 120° C for 10 minutes. The process was repeated for 4-6 times to achieve a ZnO CQDs layer thickness of ~110 nm. The resultant final thin film was annealed at 450° C for 30 minutes in a muffle furnace. Separately, solution of 1 M concentration of F8BT was prepared in chloroform. After cooling down the ZnO CQDs thin film to room temperature, thin film of F8BT (~80 nm thickness) was deposited on the ZnO CQDs film using spin coating at 1400 rpm for 40 seconds. The resultant ZnO CQDs/F8BT heterostructure was then dried at 90° C in a furnace under N_2 environment for 50 minutes. Circular dots of silver contacts of 2 mm diameter (~0.0314 cm^2 effective area of device) were grown on the F8BT layer using thermal evaporation unit (FL400 SMART COAT 3.0 A,

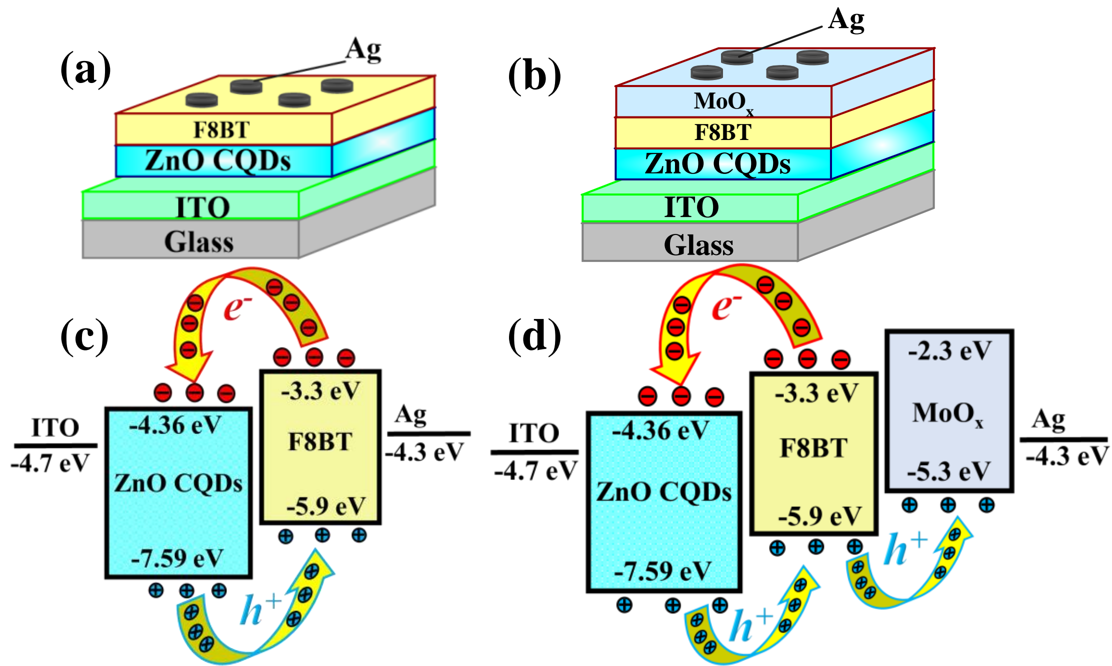

Figure 4.1. Schematic diagram of (a) Device-1 (ITO/ZnO/F8BT/Ag) (b) Device-2 (ITO/ZnO/F8BT/MoO_x/Ag) and corresponding band diagram of (c) ZnO/F8BT (d) ZnO/F8BT/MoO_x.

Hind High Vacuum, India) to prepare the ITO/ZnO CQDs/F8BT/Ag photodetector structure. For another device structure, silver (Ag) metal dots were deposited on the thin layer (~11 nm) of the MoO_x deposited on the F8BT layer by thermal evaporation method. The schematics of the two device structures under study are shown in Figure 4.1 (a) and (b) along with their energy band diagrams in Figure 4.1(c) and (d), respectively. The energies of conduction band (CB) and valence band (VB) of ZnO QDs, MoO_x and F8BT are considered to be 4.36 eV and 7.59 eV; 2.3 eV and 5.3 eV; and 5.9 eV and 3.3 eV; respectively [93], [94] [104].

4.3. Results And Discussion

4.3.1. Structural Analysis of Material (ZnO CQDs)

As discussed in Chapter 2, the TEM image (TECNAI G2 20 TWIN) shows ZnO CQDs film on a copper grid, with 20 nm and 50 nm resolution images presented. The histogram indicates an average particle size of ~2.00 nm, confirming the nanoparticle nature

of ZnO in the solution. The size of ZnO particles is below the Bohr's radius (~2.87 nm), confirming their QDs nature. The SAED image reveals diffused concentric rings, indicating a small particle size and single crystalline structure with a high surface-to-volume ratio. The d-spacing of ZnO QDs is determined as 0.262 nm and 0.146 nm for <002> and <103> orientations, respectively, using the Crystallography Open Database (COD) number 2300112 [19][20].

4.3.2. Absorption and Emission Characteristics of Thin Film

The absorbance spectra of ZnO CQDs, F8BT, MoO_x, and the combined layer of ZnO CQDs/F8BT/MoO_x are shown in Figure 4.2 (a). The dominant absorbance spectra of ZnO CQDs and F8BT layers cover the UV region and visible region, respectively. The MoO_x layer shows a very low absorbance due to its very low thickness of only ~ 11 nm. Thus, the absorbance of light in the MoOx layer is insignificant in the combined absorbance of ZnO CQDs/F8BT/MoO_x structure covering the UV-visible region. All the absorbance measurements considered here were obtained from the UV-Vis spectroscopy (V-770 from JASCO, Japan).

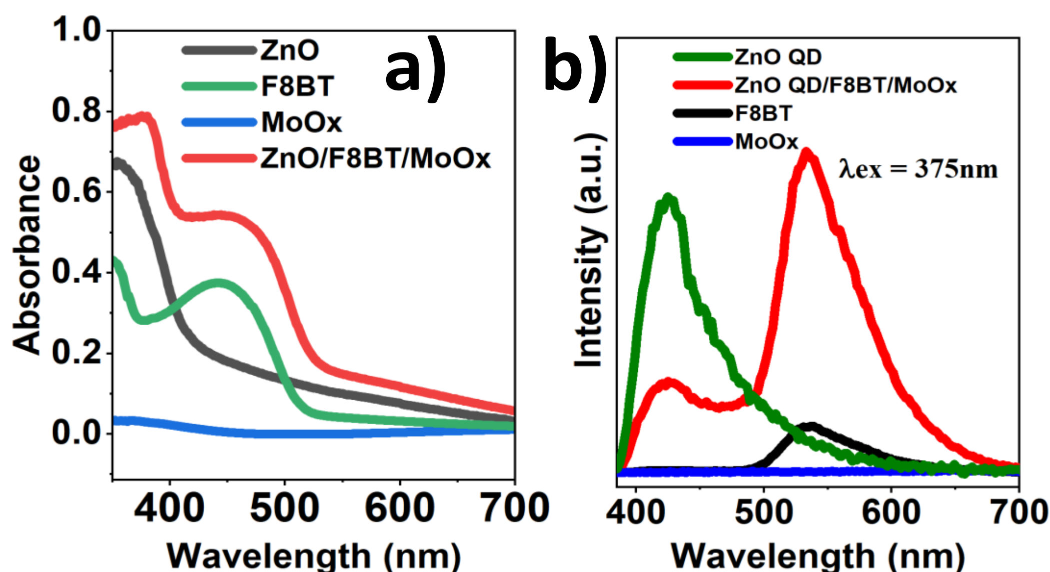

Figure 4.2 (a) Absorption spectra, and (b) Emission spectra of ZnO QDs thin film, F8BT, MoO_x and ZnO QDs /F8BT /MoO_x thin film.

The emission spectrum measurements (Edinberg Spectro fluorometer FS980) at the excitation wavelength (λ_{ex}) of 375 nm are shown in Figure 4.2 (b). The peak emission of the ZnO CQDs film was observed at ~ 440 nm whereas that of the F8BT film was observed at ~ 540 nm. No emission of the MoO_x film was observed at 375 nm at excitation. The combined emission spectra of the ZnO CQDS/ F8BT /MoO_x structure shows a reduction of the peak emission intensity peak of ZnO CQDs with the increase in the emission peak of the F8BT film. This confirms a fast energy transfer from the ZnO CQDs to F8BT in the ZnO CQDs/F8BT heterojunction material.

4.3.3. Optical Characterization

The current-voltage (I-V) characteristics of the two device structures namely ITO/ZnO CQDs/F8BT/Ag (Device-1) and ITO/ ZnO/F8BT/ MoO_x/Ag (Device-2) measured using parameter analyzer (B1500A, Keysight, USA) under dark and illumination are compared in Figure 4.3. The larger forward bias current than the reverse bias current under dark conditions (i.e., dark current) in both the devices confirm the formation of n-ZnO/p-F8BT heterojunction. The dark current and photocurrent of Device-1 are ~ 18.26 μA and ~ 74.83 μA while those of Device 2 are 0.21 μA and 48.18 μA, respectively. It may be noted that the dark current in Device-2 is much smaller than that of Device-1 due to the reduction of electron-hole recombination owing to the blocking of electrons by the MoO_x based HTL. It is interesting to note that the I-V characteristic of Device-2 under illumination shows a shift in the origin thereby confirming the photovoltaic effect. In other words, the Device-2 shows a self-powered nature.

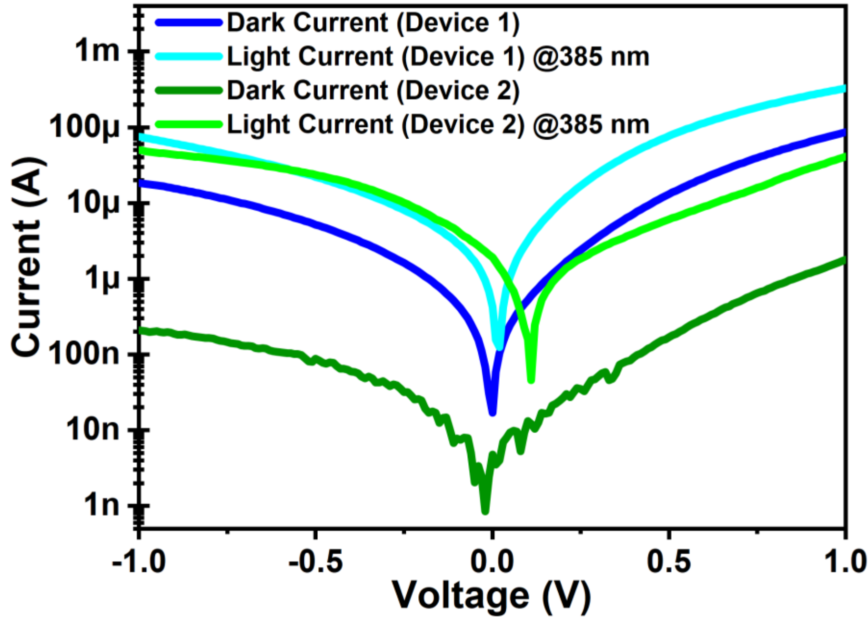

Figure 4.3 I-V characteristic of Device-1(ITO/ZnO CQDs/F8BT/Ag) and Device-2 (ITO/ZnO CQDs/F8BT/MoO_x/Ag).

The key parameters of photodetectors, namely responsivity (R), specific detectivity (D*), and external quantum efficiency (EQE), are briefly defined in the following.

The responsivity (R) is defined as the ratio of the generated photocurrent to the incident optical power at a given wavelength of incident light. The responsivity is expressed as [81][93][105]:

$$R = \frac{\text{Change in Current / Effective Area of Device}}{\text{incident Power Density on the Device}} \quad (4.1)$$

The specific detectivity (D^*) is calculated by the following equation [81][93][105]:

$$D^* = \frac{R}{\sqrt{2 \times e^- \times J_d}} \quad (4.2)$$

where, R is responsivity, e^- is the charge of an electron, and J_d is the dark current density of the detector. The EQE is defined as the ratio of the number of electrons-hole pairs collected

at external terminal to the number of photons of a particular wavelength incident on the device. The EQE is calculated as [81][93][105]:

$$EQE\ \% = \frac{1240 \times R}{\lambda\ (nm)} \times 100 \qquad (4.3)$$

where, R is responsivity, and λ is the incident wavelength in nm.

The responsivity ® and specific detectivity (D*) of Device-1 are shown in Figure 4.4 (a) and those of Device-2 are shown in Figure 4.4 (b). The responsivity ®, specific detectivity (D*) and external quantum efficiency (EQE) of the Device-1 were obtained as ~ 24 A/W, ~1.3 × 10^{12} Jones and ~7729 %, respectively, under −1 V and 25 μW/cm^2 intensity at 385 nm. Under the same operating conditions, the values of R, D* and EQE of Device-2 were ~ 44 A/W, 6.5 × 10^{12} Jones and 14171 %, respectively.

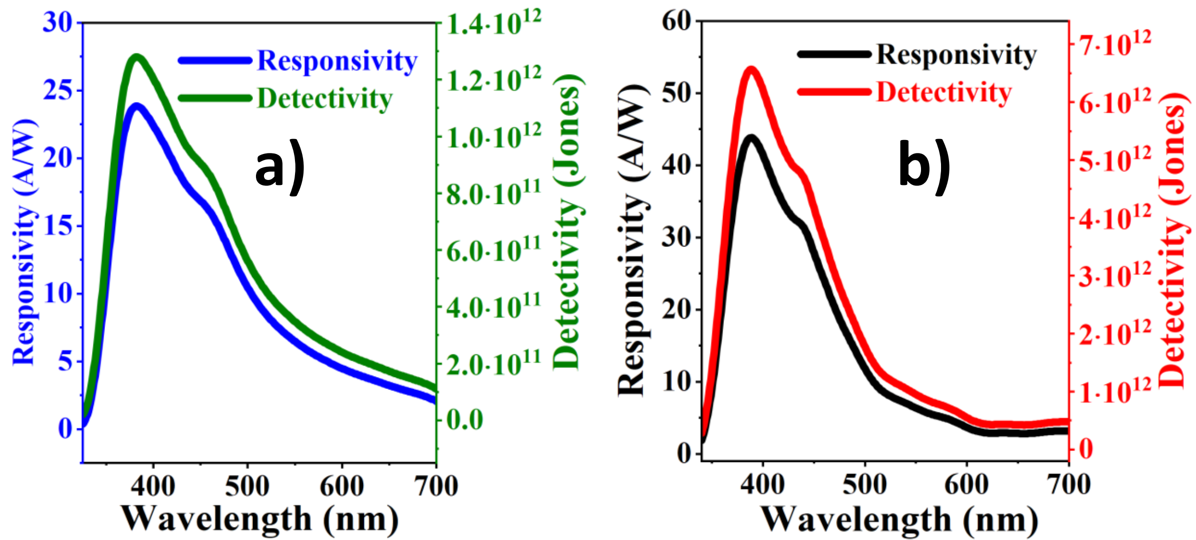

Figure 4.4 Responsivity and detectivity of (a) Device-1 (ITO/ZnO QDs/F8BT/Ag), and (b) Device-2 (ITO/ZnO QDs/F8BT/MoO_x/Ag).

The significant improvement in the performance of Device-2 is attributed to the dopant-free and hole-selective nature of MoOx HTL. Its large bandgap prevents the electrons from

entering through anode thereby reducing the electron-hole recombination in the device [81]. This, in turn, reduces the dark current and improves the overall performance of the Device-2. The EQE greater than 100 % in both the devices is attributed to the trapped charge assisted photomultiplication phenomenon [28][2]. Under the illumination condition of the reverse biased junction, some of the photogenerated electrons are trapped by the defects in the ZnO film. The coulombic charge due to these trapped electrons creates an electrostatic field which reduces the hole injection barrier at the ITO/ZnO interface. The reduced hole barrier causes an efficient hole tunneling injection from the external circuit into the active layer of the device. These trapped charge assisted tunneling of excess holes into the device enhances the photocurrent significantly, thereby causing the EQE of greater than 100 %[28][2].

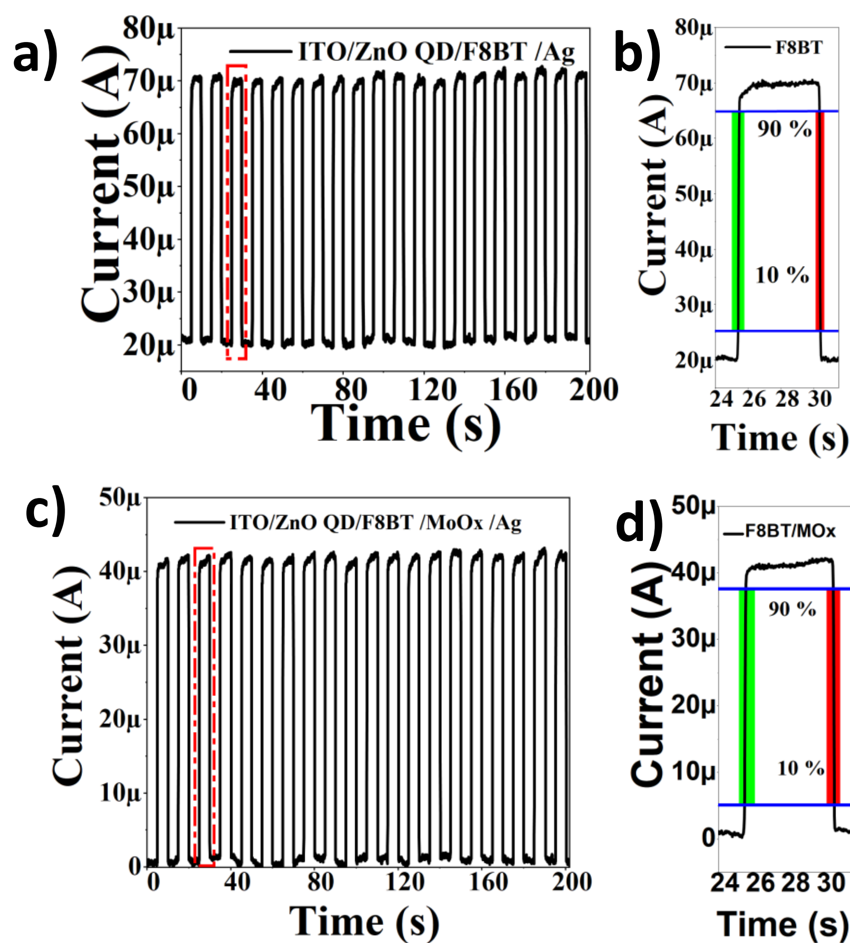

Figure 4.5 Transient response characteristics of (a), (b) Device-1 (ITO/ZnO QDs/ F8BT/Ag), and (c) and (d) Device-2 (ITO/ ZnO QDs/ F8BT/MoOx/Ag

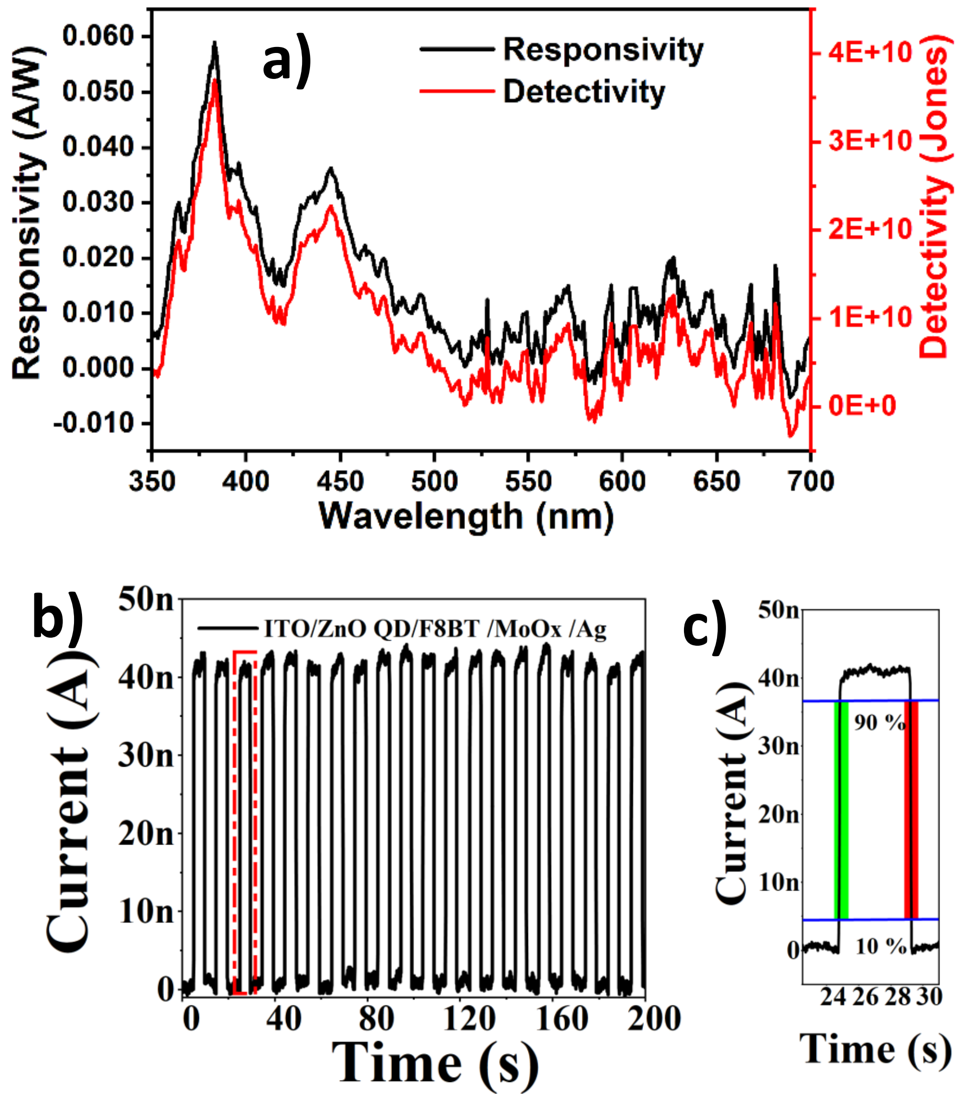

Figure 4.6 (a) Responsivity and detectivity, (b) and (c) Transient response characteristics of Device-2 (ITO/ZnO QDs/F8BT/MoO_x/Ag) at no biasing.

The response speed of any photodetector is expressed in terms of its rise time and fall time corresponding to an ON/OFF light pulse input signal. The rise time represents the time required for changing the detector current from 10% to 90% of its maximum value in response to a step change in its incident light intensity. On the other hand, the fall time

represents the time required for changing the output current from 90% to 10% of its maximum value after the light source is switched off [81][93][106]. The transient response of Device-1 and Device-2 are shown in Figure 4.5. The rise-time (τ_{on}) and fall-time (τ_{off}) of Device-1 are 0.026 s and 0.030 s, respectively, which are further improved in Device-2 as 0.016 s and 0.018 s, respectively, under 385 nm illumination of 25 μW/cm^2 intensity and -1 V bias.

TABLE 4.1: COMPARISON OF RESPONSIVITY AND DETECTIVITY OF THE PROPOSED TWO PEVICES WITH SIMILAR REPORTED DEVICES.

Device Structure	Applied Voltage	Power density (W/cm^2)	Spectral range (nm)	Responsivity (AW^{-1})	Detectivity (Jones)	Ref.
ITO / ZnO NR /P3HT / Au NPs / PEDOT:PSS /Ag	-2 V	3 m	370	17.7	-	[27]
ITO / PEDOT:PSS/F8T2:ZnO NPs / BCP / Al	-15 V	-	360 510	6.39 0.89	-	[30]
ITO / Cu2O / PVK / ZnO NR / Ag	-1 V	24.9u	360	13.28	1.03 $\times 10^{13}$	[29]
ITO / ZnO NR / P3HT / PEDOT:PSS / Ag	-2 V	3 m	370	10.7	-	[27]
ITO/interlayer / P3HT:ITIC / MoO_x / Al	-20 V	-	360	-	2.15 $\times 10^{12}$	[29]
Au/PEI-ZnO NRs/Au	-5 V	40 u	365	43.7	1.085$\times 10^{14}$	[107]
ITO/ ZnO/ PEDOT:PSS/ Ag	-8 -3	4 m 4 m	375 375	0.14 0.25	0.37 $\times 10^{10}$ 1.27 $\times 10^{11}$	[108]
ITO/ ZnO:GQD/ Poly TPD/ Ag	-3	0.59	365	0.56	2.1 $\times 10^{11}$	[109]
ITO/ZnO QDs/ F8BT/ Ag **ITO/ZnO QDs/F8BT/MoO_x/Ag**	**-1 V** **-1V**	**23u** **23u**	**385** **385**	**24** **44**	**1.3 $\times 10^{12}$** **6.5 $\times 10^{12}$**	**This Work**

TABLE 4.2: COMPARISON OF RESPONSIVITY AND TRANSIENT RESPONSE OF ZNO BASED SELF-POWERED PHOTODETECTOR.

Device Structure	R (mAW^{-1})	τ_{on} (ms)	τ_{off} (ms)	Ref.
ITO/ZNO CQDs/F8BT/Ag	**59**	**12**	**17**	**This Work**
ITO/PEDOT:PSS/F8BT/ZnO/Ag	20	36.6	37	[1]
Au/CuO /ZnO/ITO	29	80	80	[83]
B-Ga2O3/Ga:ZnO	0.76	179	275	[59]
ZnO Nrs/ Cul	86.84	110	110	[60]
ZnO/ Cul ZnO/ Cul/Au	17.7 61.5	410 410	240 80	[61]
In/PANI/Mg:ZnO/In	0.06	300	300	[62]
FTO/ZnO QD/ P3HT/MoO_x/Ag	3.04	28	200	[2]

To analyze the self-powered feature of Device-2, the responsivity and detectivity characteristics of the device measured at zero bias voltage and incident light intensity of 25 $\mu W/cm^2$ at 385 nm are shown in Figure 4.6 (a). The values of R, D* and EQE of Device-2 under zero bias condition ~ 59 mA/W, 3.70×10^{10} Jones and 18.98 %, respectively.To investigate the response speed under self-bias condition of Device-2, its transient response is shown in Figure 4.6 (b) under zero bias. The rise-time (τ_{on}) is obtained as 0.012 s and fall-

time (τ_{off}) is measured as 0.017 s which are better than their respective values under -1 V reverse bias voltage. Table 4.1 compares the responsivity and detectivity parameter values of the proposed two devices with some similar reported devices. The responsivity and transient response parameters of Device-2 under zero-bias condition are compared in Table 4.2.

4.4. Conclusion

In this chapter we have investigated the effect of HTL layer on the device with structure ITO/ZnO CQDs/F8BT/Ag. Two devices namely ITO/ZnO CQDs/ F8BT/Ag (Device-1) and ITO/ZnO CQDs/ F8BT/ MoO_x/Ag (Device-2) have been thoroughly investigated and compared in this particular chapter. The comparison results of both the fabricated device showed, the Device-2 with HTL layer showed better overall performance as compared to the device without any HTL layer. The maximum responsivity, specific detectivity and EQE measured as 44 A/W, 6.5×10^{12} Jones and 14171 %, respectively. While in the visible region at 450 nm device without the MoO_x layer showed a maximum responsivity of 16.86 A/W, while the one with the MoO_x layer showed a responsivity of 27.89 A/W. The detectivity of the device at 450 nm improved from 9.05×10^{11} Jones to 4.17×10^{12} Jones on insertion of the MoO_x layer. The enhancement in the device performance with MoO_x HTL layer in Device-2 is attributed to better band tunning. Additionally the self-powered feature is also introduced in the device 2. The rise-time and fall-time of Device-1 and Device-2 were measured as 0.026 s and 0.030 s; and 0.016 s and 0.018 s; respectively. Interestingly, The rise-time and fall time of Device-2 under self-bias (i.e. zero external bias) condition were measured as 0.012 s and 0.017 s respectively.